Micro-Optics for Liquid Crystal Displays Applications

Han-Ping D. Shieh, Yi-Pai Huang, and Ko-Wei Chien

Invited Paper

***Abstract*—Micro-optics have become the key technology in liquid crystal display systems due to its capabilities of miniaturization and design flexibility. Design consideration and experimental results of microoptical components for enhancing the image quality, providing better functions, increasing light efficiency, and generating 3D images in liquid crystal display (LCD) applications are presented.**

***Index Terms*—Cholesteric, focusing foil, grooved lightguide, image-enhanced reflector, light control film, microlens array, micro-tube array, random grating, sub-wavelength grating, three-dimensional (3-D) display, transflective.**

I. Introduction

MICRO-OPTICS have emerged as a new branch of science during the past 10–20 years and is gradually making its way toward commercialization in a number of fields. It is a key technology to meet the needs of miniaturization, cost reduction, and enhanced performance. Micro-optics is also a quintessential enabling technology for various electro-optical systems, as shown in Fig. 1, which has become the important technique for building compact optoelectronic system. Especially in electronic display systems, microoptical components contribute various novel devices that bring more flexibility in system design to increase the overall performance, thus, offering more appealing display devices.

Traditional passive optical components are used to collect, redistribute, or modify optical radiation. Refractive and reflective components, such as lens, prism, and mirrors are well known, and already have been used for centuries. Micro-optics [1], enabling the collection, distribution, or modification of light, is an effective method to shape and influence light with very small

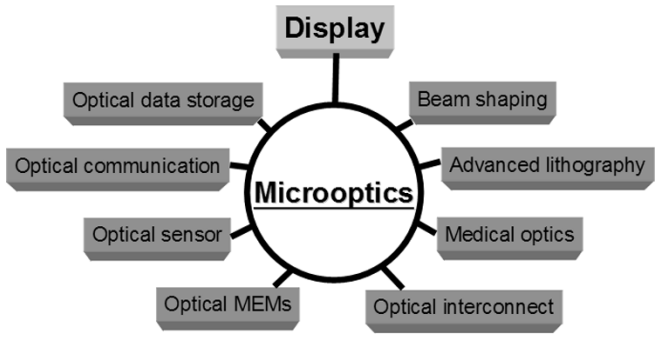

Fig. 1. Applications of micro-optics.

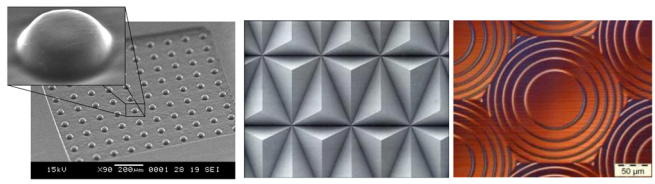

Fig. 2. Microoptical components. (a) Microlens. (b) Microprisms. (c) DOEs. (Color version available online at http://ieeexplore.ieee.org.)

structures and components. Liquid-crystal displays (LCDs) [2] are light-controlling devices, which rely on the optical properties of liquid-crystal materials to control the output light from an external light source. Among LCDs, reflective/transflective types become popular technologies for mobile and low-power applications under ambient illumination. Micro-optics is a key technology to further improve the performance, minimize the size, and reduce the cost to meet the demanding requirement of portable LCDs.

Micro-refractive optical components, such as microlens [Fig. 2(a)] and micro-prism [Fig. 2(b)] with diameter of 1 mm to a few micrometers, can now be fabricated with high quality, using techniques such as graded-index [3], [4], photo-thermal [5], thermal reflow, and photoresist 'sculpture'. Likewise, typical diffractive optical elements (DOEs), as shown in Fig. 2(c), of multilevel micro-relieves (binary optics) or continuous relief and amplitudes of a few micrometers also achieve the similar functions of those of micro-optics. Following the development of micro-fabrication fabrication methods and the associated tooling technologies, various fabrication methods, such as VLSI lithography/patterning/etching techniques, laser writing,

Manuscript received February 19, 2005; revised April 8, 2005. This work was supported by NSC93-2215-E009-72 project, MOEA Technology Development Program for Academia on Display and National Chiao Tung Univeristy (NCTU) Display Research Center, and by the National Chiao Tung University (NCTU) Display Research Center.

H.-P. D. Shieh is with the Department of Photonics and Display Institute, National Chiao Tung University, Hsinchu 30010, Taiwan, R.O.C. (e-mail: hpshieh@mail.nctu.edu.tw).

Y.-P. Huang was with the Department of Photonics and Display Institute, National Chiao Tung University, Hsinchu 30010, Taiwan, R.O.C. He is now with AU Optronics, Hsinchu 300, Taiwan, R.O.C. (e-mail: BoundsHuang@auo.com).

K.-W. Chien is with the Department of Photonics and Institute of Electro-Optical Engineering, National Chiao Tung University, Hsinchu 30010, Taiwan, R.O.C. (e-mail: dodu.eo88g@nctu.edu.tw).

Digital Object Identifier 10.1109/JDT.2005.852504

and plastic molding, etc., have been developed to fabricate the DOEs for practical applications. Almost any structure and shape, including asymmetric sphere, can be fabricated, providing high degree of flexibility for design. Moreover, DOEs are in the form of planar structure, resulting in more versatile applications and system integration.

In this paper, design consideration and experimental results of microoptical components for enhancing the image quality, providing enhanced functionality, increasing light efficiency, and generating 3-D images in LCD applications will be presented and demonstrated.

II. Principle of Microoptical Components

Most classical macrooptical components, such as lens, prism, and mirror, are designed using the theory of geometrical optics, treating light as geometrical rays which are refracted and reflected at optical interface, for example, between air and glass, as described by Snell's law. However, such a structure is not easily fabricated in microstructure, especially in the dimensions of a few microns. Therefore, in the 1970s and 1980s, planner DOEs were developed. DOEs have several advantages. They: 1) allow manipulating light fields in ways that would be difficult by traditional refractive and reflective optics; 2) can be inexpensive and light weight; and 3) are more flexible in the design process.

To determine the optical path and efficiency of light transmitting in DOEs, scalar and vector diffractions are two main theories used in the design. Vector diffraction theory is a rigorous electromagnetic theory, where light is treated as electromagnetic wave, and the propagation in optical system is derived by Maxwell equations. However, in most cases, the numerical computing is prohibitively time consuming. In contrast, scalar diffraction theory is simple and efficient in calculation. However, scalar diffraction theory, derived from the Fourier optics, cannot deal with the phenomenon of polarization. In addition, scalar diffraction theory is only applicable for the large scale microstructure; namely, the variation of the surface-relief or index-modulation profile is larger than the wavelength of light λ, or the aspect ratio (depth/width) is close to λ [6]. Fortunately, most microoptical elements are not so small in feature dimension, hence, the scalar diffraction theory is adequate to deal with most functions of DOEs [7].

A. Binary Micro-Gratings

Binary grating elements have the stepped approximation with respect to an ideal continuous phase profile. Diffraction efficiency of binary microoptical component depends on the number of steps in this staircase-like binary optical element. The continuous blazed grating, shown in Fig. 3, make it possible for 100% of incident light diffracted into a single first diffraction order if the peak-to-peak variation introduces exactly 2π rad. The binary optic approximation to grating is a quantized version with 2^N-levels. If there are 2^N steps of equal spaces and thickness existed in one period, one micro prism in grating, of this blazed phase grating, the thickness of the nth step is

$$d_n = n \cdot d_1 = n \cdot \frac{\Delta_0}{2^N} \tag{1}$$

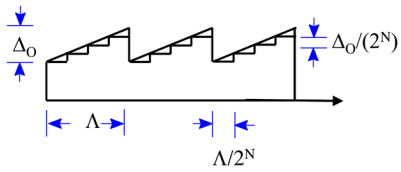

Fig. 3. Ideal sawtooth thickness profile for a blazed grating and binary optical approximation to that profile. (Color version available online at http://ieeexplore.ieee.org.)

where Δ_0 is the peak-to-peak thickness of the blazed grating. If n_s denotes refraction index of the grating substrate, and λ denotes wavelength of light in air, the phase retardation of each step is expressed as

$$\varphi_n = \frac{2\pi}{\lambda}[n_s - 1] \cdot d_n. \tag{2}$$

Thus, the diffraction efficiency of this step approximation can be obtained by expanding its periodic amplitude transmission in a Fourier series. From these calculations, the diffraction efficiency (η) of qth diffraction order can be expressed by

$$\eta_q = \sin c^2\left(\frac{q}{2^N}\right) \frac{\sin c^2\left(q - \frac{\Phi_0}{2\pi}\right)}{\sin c^2\left(\frac{q - \frac{\Phi_0}{2\pi}}{2^N}\right)} \tag{3}$$

where Φ_0 is the peak-to-peak phase difference of this blazed grating, and is related to the peak-to-peak thickness variation through

$$\Phi_0 = \frac{2\pi(n_s - n_o)}{\lambda}\Delta_0 \tag{4}$$

where n_0 is the refraction index of the surrounding.

Of special interest is the case of a quantized approximation to the blazed grating with a peak-to-peak phase difference of $\Phi_0 = 2\,\pi$, yielding

$$\eta_q = \sin c^2\left(\frac{q}{2^N}\right) \frac{\sin c^2(q-1)}{\sin c^2\left(\frac{q-1}{2^N}\right)}. \tag{5}$$

Therefore, diffraction efficiency of the primary order of interest, namely, the $+1$ order $(\mathbf{q} = 1)$, is

$$\eta_1 = \sin c^2\left(\frac{1}{2^N}\right). \tag{6}$$

The primary $+1$ order diffraction efficiency increases with the number of step (2^N), reaching 81% for a four-level grating and 95% for an eight-level grating.

The classical diffraction grating function can be taken to calculate the diffraction angle, as described by the following grating equation:

$$\sin\theta_2 = \sin\theta_1 + m\lambda/\Lambda \tag{7}$$

where Λ is the period of grating and m is the diffraction order.

B. Fresnel Microlens

If the phase quantization procedure described above is applied to the circularly symmetrical phase profiles of microlens,

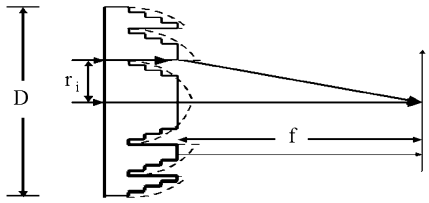

Fig. 4. Diffraction microlens of continuous and binary phase structure.

it yields a set of annular rings which are typical for diffractive lenses. This annular ring structure is designed based on the Fresnel zone plate (FZPs) theory. The ring system consists of continuous phase function or binary phase function structures to achieve whole phase diffraction elements. In both cases, the annular rings are designed such that the optical path lengths for the light deflected from adjacent zones toward a common focal point differ by an integral multiple of a design wavelength, as shown in Fig. 4. If r_i and f denote the radius of the i-th ring and the focal plane, respectively, this condition is expressed mathematically as [8]

$$\mathsf{r}_i^2 + \mathsf{f}^2 = (\mathsf{f} + \mathsf{i}\lambda)^2. \tag{8}$$

Thus, the radius r_i of the ith zone follows that

$$\mathsf{r}_i^2 = 2\mathsf{i}\lambda\mathsf{f} + (\mathsf{i}\lambda)^2. \tag{9}$$

To meet this condition, the phase function $\Phi(x, y)$ of the binary Fresnel microlens is rewritten as

$$\Phi(x, y) = \Phi(r^2) = \Phi\left(r^2 + K * r_p^2\right) \tag{10}$$

where K is an integer, $r_p^2 = 2\lambda\mathsf{f}$ is the period, and λ is the design wavelength. As $\Phi(x, y)$ is a periodic function, it can be expanded into Fourier series:

$$\Phi(r^2) = \sum_{m=-\infty}^{\infty} A_m e^{(j2m\pi\frac{r^2}{r_P^2})} \tag{11}$$

where A_m is the coefficient of Fourier series, namely the amplitude of each diffraction order

$$A_m = \frac{1}{r_P^2} \int_0^{r_P^2} \Phi(r^2) e^{(-j2m\pi r^2)} dr^2. \tag{12}$$

From the L-level quantized phase profile shown in Fig. 4, the phase function of this binary Fresnel lens is rewritten as

$$\Phi(r^2) = \sum_{k=0}^{N(L-1)} \exp\left(-\frac{j2\pi k}{L}\right) * \mathrm{rect}\left(\frac{r^2 - \frac{kr_p^2}{L} - \frac{r_p^2}{2L}}{\frac{r_p^2}{L}}\right) \tag{13}$$

Substituting (14) into (13) yields the amplitude function as

$$\begin{aligned} A_m &= \sum_{k=0}^{N(L-1)} \exp\left(-\frac{j2\pi k}{L}\right) \int_{k/L}^{k+1/L} \exp(-j2\pi m x)\, dx; \\ \text{set } x &= \frac{r^2}{r_p^2} \\ &= \sum_{k=0}^{N(L-1)} \exp\left(-\frac{j2\pi k}{L}\right) \\ &\quad * \frac{1}{j2\pi m} * \exp\left(-j2\pi m \frac{k}{L}\right) \left[1 - \exp\left(-j2\pi \frac{m}{L}\right)\right] \\ &= \exp\left(-\frac{jm\pi}{L}\right) * \sin c\left(\frac{m}{L}\right) \\ &\quad * \frac{1}{L} * \sum_{k=0}^{N(L-1)} \exp\left[-\frac{j2\pi k(1+m)}{L}\right] \end{aligned} \tag{14}$$

Observing (14), we can get

$$\begin{aligned} &\sum_{k=0}^{N(L-1)} \exp\left[-\frac{j2\pi k(1+m)}{L}\right] \\ &\qquad = \begin{cases} L, & \text{when } m = I * L - 1, \quad I = \text{integer} \\ 0, & \text{others} \end{cases} \end{aligned} \tag{15}$$

In order to enhance the intensity of focused light, this diffractive lens is optimized in certain diffraction orders. From the above discussion, we use the -1 order diffraction to design the binary Fresnel lens. The diffraction efficiency is normalized by

$$\eta_{-1} = \frac{I_{-1}}{\sum_{m=-\infty}^{\infty} I_m} = \sin c^2\left(\frac{1}{L}\right) \tag{16}$$

We obtain similar diffraction efficiency equations of diffractive grating (6) and diffractive lens (16). Exactly, the diffractive lens structure can be considered as an annular grating with varying periods for reflected light focusing. In the central part of lens, the grating periods are larger, therefore, the quantization of the phase profile into more levels (>8) is simple and not critical. However, the grating periods become smaller toward the rim. The number of the phase levels is limited by the resolution of fabrication process, such as VLSI lithography. This limitation in fabrication also restricts the F-number of diffractive lens as

$$\Delta R_{\min} = R_m - R_{m-1} = \frac{\lambda}{2} \cdot \frac{f}{D} = \frac{\lambda}{2} \cdot (F/\#). \tag{17}$$

III. Fabrication of Surface Relief Microoptical Components

Making microoptical elements by creating a surface relief pattern is presently a common practice of micro-optics. Due to multitude of applications for surface relief microoptical components, a range of materials, pattering techniques and actual

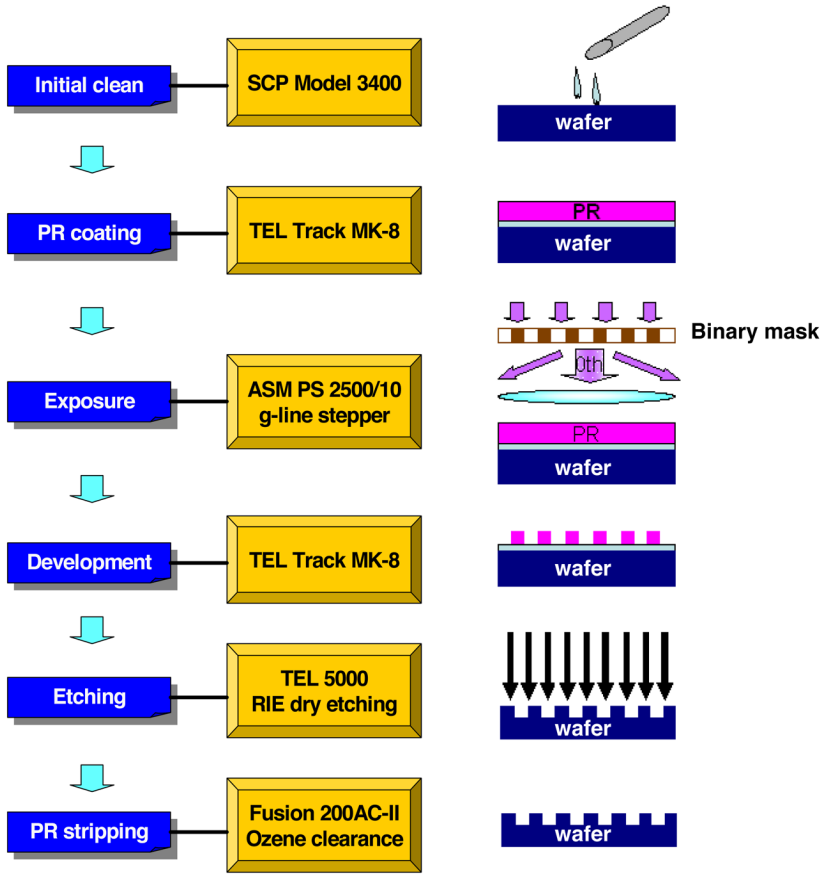

Fig. 5. Detail processes of lithography and etching to realize the technology of half-tone mask. (Color version available online at http://ieeexplore.ieee.org.)

relief fabrication tools are available. For the continuous and binary surface relief structures, there are different pattern designs and fabrication processes, respectively.

Except direct tooling techniques, all these processes are similar to the VLSI fabrication processes. The patterning processes include normal lithography/direct writing to produce the binary pattern on the photoresist (PR) layer. After the development, the desired features are patterned on PR layer. Then the fabrication processes transfer the structure from PR to the substrate. However, for the continuous surface relief optical components, the e-beam/laser direct writing with the thermal reflow and gray-tone mask technology are developed for different applications.

The selection of the most suitable material for each specific application depends on the required performance and cost of microoptical device. Polymers with the molding fabrication process have been considered for low cost and high volume replication, thus setting an upper limit to optical precision and performance, such as surface uniformity and substrate birefringence. If low volume products is involved, a broad range of materials, such as silica glass, quartz, bulk plastic, or thin film deposited on a transparent substrate, are available.

A. Semiconductor Process and Plastic Replication for Binary Relief Optical Components

The fabrication process to produce a microoptical structure on Si-wafer includes mask generating, lithography, and etching is similar to VLSI fabrication processes. An example of the process is illustrated in Fig. 5.

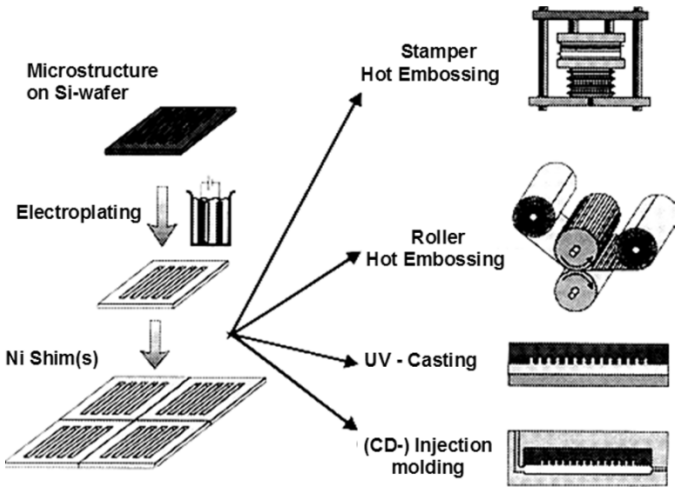

Fig. 6. Replication processes and the corresponding techniques.

The above process is suitable for generating the microoptical structure on Si-wafer. However, for the cost concern and mass production, replication is necessary. Fig. 6 illustrates an overview of the major replication technologies. To replicate the original structure on Si-wafer, a Ni shim is formed by electroplating as a master. From this first Ni master, second and third generation masters can be formed. The stamper hot embossing and roller hot embossing are well-established technologies for

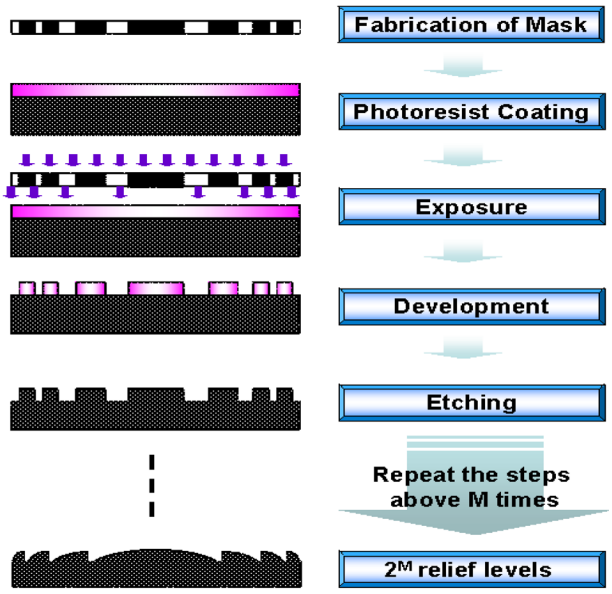

Fig. 7. Flow of the traditional multibinary mask lithography. (Color version available online at http://ieeexplore.ieee.org.)

replication of surface relief elements with depths up to ~1 μm. Deeper structures can be replicated as well by UV-casting or injection molding, which have demonstrated good results for elements with a minimum segment size of 5 μm and a relief depth of 5 μm.

The light control films presented in this paper were fabricated by using the mentioned techniques. Utilizing a standard VLSI process, the binary pattern of designed structure is generated on a Si wafer. Then the patterns are economically replicated on a 100-μm thick plastic thin foil using the stamper hot embossing.

B. Half-Tone Mask by Excimer Laser Micromachining for Continuous Relief Structures

Conventional well-developed VLSI technology uses a set of sequential binary masks to build up discrete phase levels of micro-optics. M binary masks can produce 2^M binary relief levels by means of successive photoresist spinning, exposure, development, etching steps, as shown in Fig. 7. Nevertheless, due to the limitation of alignment accuracy, the error introduced from alignment, coating, exposure, development, and etching increase rapidly with the increase of the mask number, thus degrading efficiency of the device.

Half-tone mask technology is a binary mask whose critical dimension is of smaller than the resolution limit of the optical exposure system. Gray levels are encoded through the density and diameter of binary structure, as shown in Fig. 8. The continuous profiles are achievable through this technique by using only one mask, hence, great potential for mass fabrication cost-effectively.

IV. Micro-Optics for LC Displays

Design flexibility is one of the advantages of micro-optics. We presented various microoptical structures for demanding display applications: 1) multidirectional asymmetrical microlens array light control films (MAMA-LCF) and random

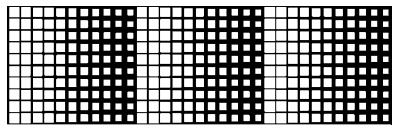

Fig. 8. Coded half-tone masks.

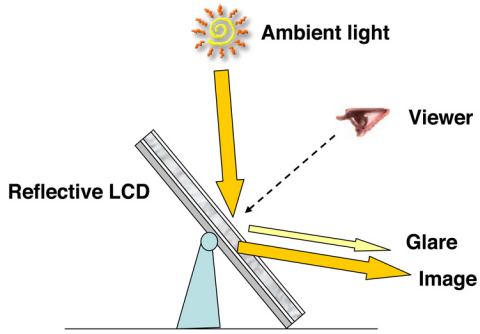

Fig. 9. Typical office illumination and the reflected light distribution of reflective LCDs. (Color version available online at http://ieeexplore.ieee.org.)

grating light control films [12], [13] for increasing the brightness of reflective images; 2) image-enhanced reflector (IER) for achieving "transflective" cholesteric LCDs; 3) microtube array for improving the backlight utilization of transflective LCDs; 4) sub-wavelength grating [17] for doubling the backlight efficiency; and 5) grooved-lightguide with focusing foil [19] for generating 3-D images. We will use MAMA-LCF as an example to illustrate the issues of color dispersion, moiré effect, surface scattering and lamination of very thin microoptical foils on LCDs. The detailed design and experimental results are described in the following.

A. Microoptics in Portable LCDs

Low brightness and poor contrast ration (CR) are among two major issues for reflective LCDs, and inadequate transmittance and unmatched color saturation are the disadvantages for transflective ones. Therefore, microoptical components, which meet the needs of miniaturization and performance improvement, bring various novel optical designs to enhance the image quality for portable LCDs.

1) Microoptics in Reflective LCDs: Conventional reflective LCDs with metallic reflectors reflect modulated light for viewing. Under oblique illumination, the specular reflection of planar reflector reflects the oblique incident light to its corresponding reflection angle. Consequently, the viewers cannot perceive the brightest image near the normal direction, a typical viewing region for common viewers, as shown in Fig. 9. Moreover, the brightest reflected image is at the glare angle where surface reflection from the front glass interferes with image, thus, degrades the contrast.

Many methods have been reported for improving the brightness and CR of reflective LCDs. The two successful methods of micro-optics in reflective LCDs are rough surface reflector [9] and microslant reflector (MSR) [10]. Rough surface reflector as depicted in Fig. 10(top), implemented on the inner side of the rear substrate can scatter the reflective light into wider viewing region. Therefore, the observers see brighter image

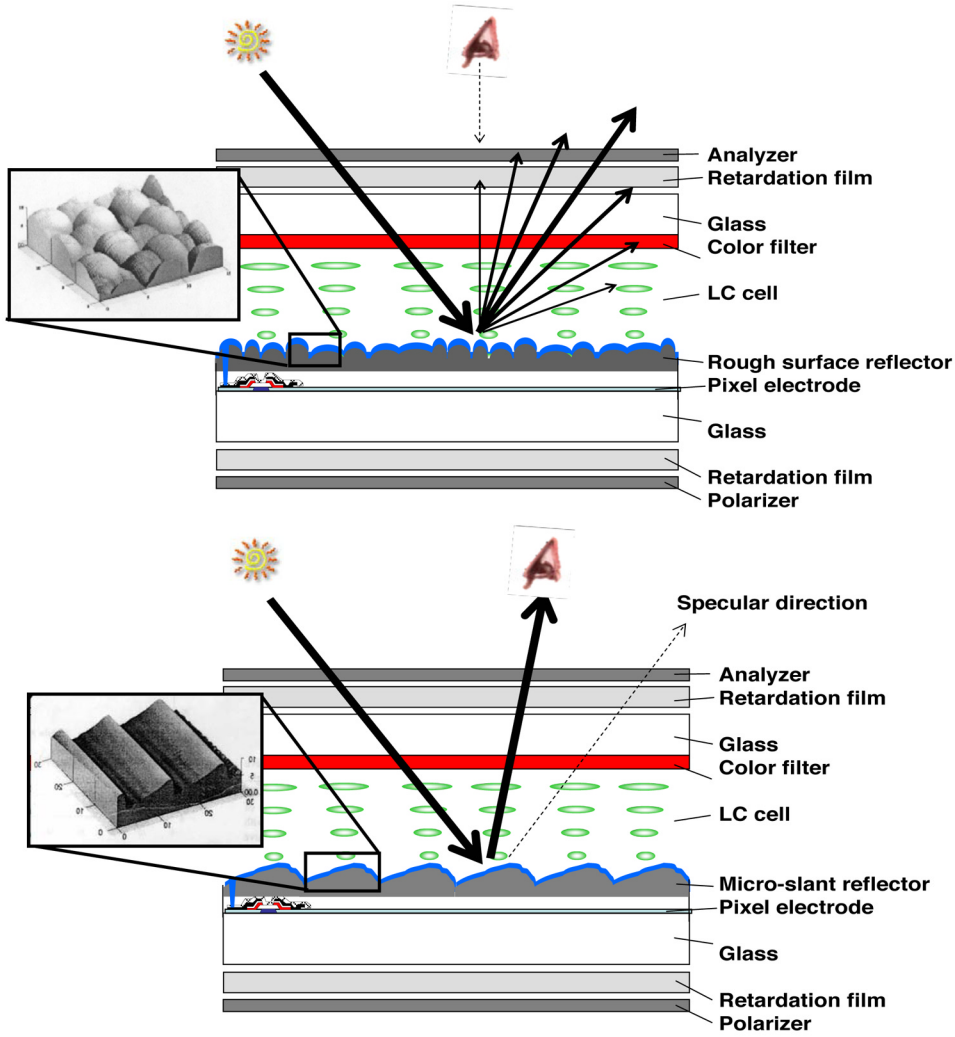

Fig. 10. Optical configuration of a reflective LCD with (top) rough surface reflector and (bottom) MSR. (Color version available online at http://ieeexplore.ieee.org.)

in the normal direction. Additionally, the TFT structures are hidden beneath the reflector. Thus, the aperture ratio is greater than 90%, and can further increase the brightness. The MSR, as shown in Fig. 10(bottom), is formed as an asymmetrical slant reflector, which can shift the peak of the reflected light away from specular direction by $\sim 12^{\circ}$. Therefore, CR in the range 20–30:1 has been achieved. Due to the optical gain, the reflectance normal to the surface is about 0.4X over the MgO standard white, a factor of 4 brighter than an LC cell with a mirror reflector.

Many methods, for example, laminating front scattering film on color STN-LCDs, building rough surface reflector (bump reflector) on the bottom substrate of PDLC, and using single surface rubbed cell for Ch-LCDs, have been proposed for improving the brightness and the contrast ratio. An unidirectional asymmetrical microlens array light control film (AMA-LCF) [11] had been proposed to enhance the brightness of reflective LCDs. AMA-LCFs constructed by cutting in the direction of the microlens array diameter to form an off-axis array and then laminating it onto the front surface of reflective LCDs, are effective yet low in cost. As shown in Fig. 11, oblique incident light can be reflected to a near-normal viewing zone, yielding significant gain in brightness, and thus, enhanced image quality.

However, the AMA-LCF fabricated was for unidirectional ambient illumination. The brightness and CR enhancement decrease if the light source is not illuminated from the designed direction. Therefore, the concept of AMA-LCF was extended to multidirectional asymmetrical microlens array light control film (MAMA-LCF) [12], [13] and random grating light control film (RG-LCF) so that multiple ambient illuminations can be effectively collected and redirected. MAMA-LCF can focus the reflected light in a specific viewing angle and yield ultra high brightness image with high CR. By optimizing the grating pitches and orientations of RG-LCF, the reflective light distribution can be well controlled and results in high brightness, wide viewing angle, and high uniformity images. Light control films are also applicable to other modes of reflective LCDs: color STN-LCD, PDLC, and Ch-LCD.

B. Optical Design of Multidirectional AMA-LCF

Multidirectional AMA-LCF (MAMA-LCF) with a fill factor of 100% was designed for a typical ambient environment to significantly improve image quality. In addition to high ambient light utilization, laminating the MAMA-LCF onto various reflective displays can also yield a wide light-collecting angle.

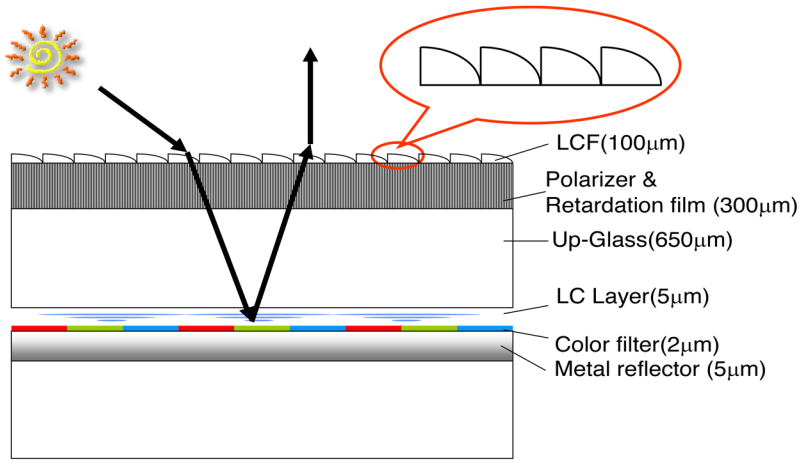

Fig. 11. Panel configuration of a reflective display laminating a light control film for collecting and redirecting ambient illuminations. (Color version available online at http://ieeexplore.ieee.org.)

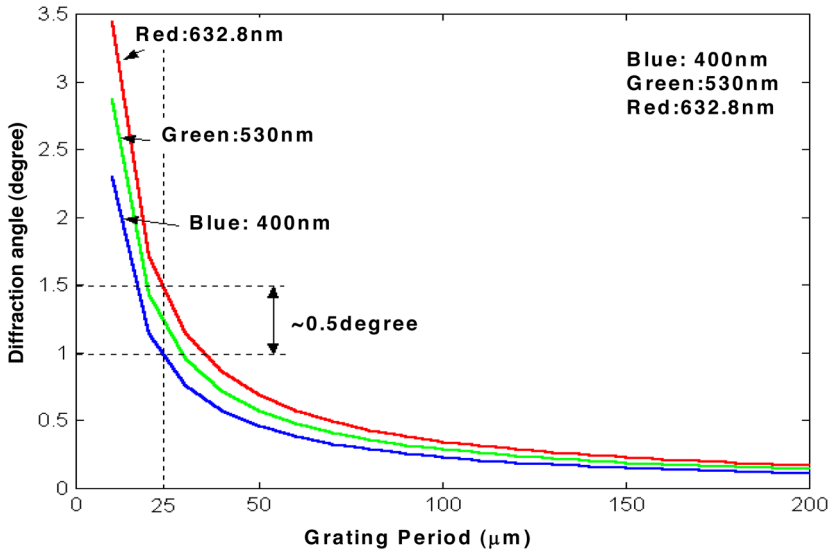

Fig. 12. Simulated results of color dispersion. (Color version available online at http://ieeexplore.ieee.org.)

To avoid color dispersion, the MAMA-LCF structure was modeled as multiple slit gratings of aperture width $\mathbf{b}$ and pitch $\mathbf{h}$. Furthermore, color dispersion should be considered in terms of diffraction angle and intensity, which can be calculated from (18) and (19)

$$n\lambda = h\sin\theta \quad \text{for } n = 0, \pm 1, \pm 2, \ldots. \tag{18}$$

Here, $\boldsymbol{n}$ denotes the order of diffraction and θ is the angle of diffraction. The relationship between wavelength and diffraction angle can be defined from (18). A diffraction intensity, $\boldsymbol{I}$ of different order is then derived using

$$I = I_0 \left(\frac{\sin\beta}{\beta}\right)^2 \left(\frac{\sin N\gamma}{N\sin\gamma}\right)^2 \tag{19}$$

where I_0 is the zeroth-order diffraction intensity, $\beta = 1/2kb\sin\theta$ and $\gamma = 1/2kh\sin\theta, \theta$ is the diffraction angle which can be derived from (18), and $\boldsymbol{k}$ is the wavenumber $2\pi/\lambda$. The factor $\boldsymbol{N}$ renders $\mathbf{I} = \mathbf{I}_0$ when $\theta = 0$. Therefore, by comparing the intensity of different diffraction orders, we can determine which order is relevant, and then (19) can be used to derive the dispersion angle. Accordingly, the human pupil and the viewing distance determine the minimum grating period of indistinguishable color dispersion, and are taken into account in the design of MAMA-LCF.

We assumed the human pupil to be 3 mm in diameter and the viewing distance to be 30 cm, therefore, the difference in the red (R), green (G), and blue (B) diffraction angles should be, at most, 0.573°. The three curves shown in Fig. 12 depict the diffraction angle for three different wavelengths and grating periods where the grating period of less than 25 μm may cause a difference in the R, G, and B diffraction angle of larger than 0.5°, resulting in visible dispersion. Accordingly, the minimum grating period of MAMA-LCF is 25 μm.

The moiré pattern, which might occur when periodic LCF structures and periodic pixels of a color filter are superimposed, was also considered by adopting a specific ratio of the periods of those two structures with a fixed angular difference, which can be calculated by the following equations:

$$q_1 = f_2/f_1 \tag{20}$$

$$\begin{pmatrix} f_u \\ f_v \end{pmatrix}_{k_1,k_2} = \begin{pmatrix} \cos\alpha & -\sin\alpha \\ \sin\alpha & \cos\alpha \end{pmatrix} \begin{pmatrix} k_1 \\ 0 \end{pmatrix} f_1 + \begin{pmatrix} k_2 \\ 0 \end{pmatrix} q_1, f_1 \tag{21}$$

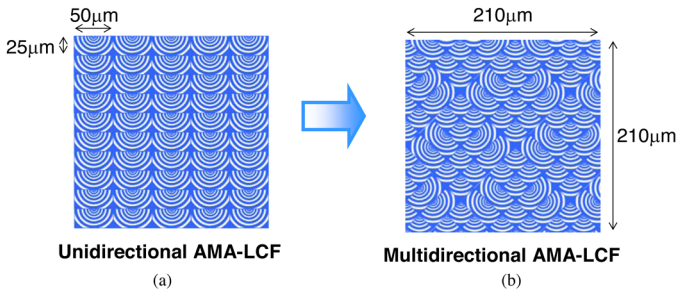

Fig. 13. Plane view of (a) unidirectional and (b) multidirectional AMA-LCFs for a color STN-LCD of pixel size of 25×50 μm. (Color version available online at http://ieeexplore.ieee.org.)

where f_2 and f_1 are the frequencies of the periodic patterns on the color filter and MAMA-LCF, respectively. The vector (f_u, f_v) denotes the spatial frequency required for the moiré pattern to occur. The angle α is the angular difference between two structures, and (k_1, k_2) are the harmonic terms of each frequency. Thus, the frequency f_{k_1,k_2} and the period T_{k_1,k_2} at which the moiré pattern occurs are given by the sum vector f

$$f_{k_1,k_2} = \sqrt{f_{u_{k_1,k_2}}^2 + f_{v_{k_1,k_2}}^2} \tag{22}$$

$$T_{k_1,k_2} = \frac{1}{f_{k_1,k_2}}. \tag{23}$$

The human eyes cannot resolve the moiré pattern with a period of less than 1. Because the frequency of the color filter (f_2) is fixed, the non-moiré frequency (f_1) and the orientation (α) of MAMA-LCF can be derived from (20) to (23). Then, MAMA-LCF can be designed to have microlenses with multiple orientations, where each microlens has different pitch and orientation [14].

Therefore, the MAMA-LCF shown schematically in Fig. 13(b), whose microlenses are rotated in three different orientations $(0^\circ, \pm 45^\circ)$ and rearranged into a particular structure, was designed and fabricated. The superimposition of a unidirectional LCF and a color STN-LCD caused several undesirable oblique strips, i.e., moiré patterns, have been successfully eliminated by using the new MAMA-LCF. Additionally, to be applicable to a reflective color STN-LCD with pixel size with 210 μm $\times$ 210 μm, there are more than 50 microlenses within each pixel. Thus, moiré patterns are not visible as the designed structure and the pitch of the microlenses are much smaller than the pixel size.

C. Surface Scattering

From Fresnel equation and Snell's law, the surface reflective ratio [14] between two layers with different refractive index for S wave (TE) and P wave (TM) can be, respectively, shown as

$$\begin{aligned} R_s &= |r_s|^2 \\ &= |(\cos\theta - \sqrt{n^2 - \sin^2\theta})/(\cos\theta + \sqrt{n^2 - \sin^2\theta})|^2 \end{aligned} \tag{24}$$

$$\begin{aligned} R_p &= |r_p|^2 \\ &= -|(n^2\cos\theta + \sqrt{n^2 - \sin^2\theta})/ \\ &\qquad (n^2\cos\theta + \sqrt{n^2 - \sin^2\theta})|^2. \end{aligned} \tag{25}$$

Here $n = (n_t/n_i)$is the relative refractive index of refraction of the refractive index of the incident (n_i) and the transmitted (n_t) media, and θ is the light incident angle. Therefore, the total surface reflective ratio R_{total} is

$$R_{\text{total}} = \sqrt{(I_{is} \cdot R_s)^2 + (I_{ip}) \cdot R_p)^2}/\sqrt{(I_{is}^2 + (I_{ip})^2} \tag{26}$$

where $\mathrm{I_{is}}$ and $\mathrm{I_{ip}}$ are the intensities of the incident S and P wave, respectively. Assuming the incident light is unpolarized, then $\mathrm{I_{is}} = \mathrm{I_{ip}}$. Consequently, $\mathrm{R_{total}}$ can be simplified to be:

$$R_{\text{total}} = \sqrt{(R_s)^2 + (R_p)^2}/\sqrt{2} \tag{27}$$

For example, while the light illuminated on a plastic film of refractive index $n = 1.55$ from 30°, the total surface reflection is 5.15%. Compared to the 12.5% reflective light efficiency of a reflective LCD, as signified in Fig. 14, the surface reflection results in very serious degradation to the CR. Additionally, the microlens on MAMA-LCF was approximated by using a four-step Fresnel lens instead of traditional curvature lens. Therefore, the edge of each step may scatter the incident light, which results in increased dark state light leakage and degraded CR.

D. Reflective LCDs With MAMA-LCF

Several methods were proposed, respectively, for laminating the LCF on the following three different kinds of LCDs: reflective color STN, PDLC, and cholesteric, to overcome the above-mentioned issues. Coating an index matching material on LCF and laminating it below the polarizer, as depicted in, is found to greatly reduce the intensity of interface reflection and front scattering light. As a result, MAMA-LCF laminated below the polarizer should be made of a very low birefringence material to avoid the color shift caused by the retardation effect. MAMA-LCF is preferred to be laminated between the bottom substrate of the plastic PDLC panel and the aluminum reflector with an index matching material coated, as depicted in Fig. 15 to avoid deteriorating the blackness of the dark state. Moreover, the plastic LCF is flexible and can be easily combined with the plastic PDLC displays.

Integrating a MAMA-LCF on the two-surface rubbed cell to control viewing angle while preserving high reflectivity shall be more appealing for cholesteric liquid crystal display (Ch-LCD) applications. As shown in Fig. 16, the MAMA-LCF helps to direct light to a normal viewing angle. Moreover, by coating an index matching material can reduce the interface reflections. Benefited from the light control film, the two-surface rubbed Ch-LCD is expected to exhibit high reflectivity in normal viewing direction.

E. Image Quality Enhancement by MAMA-LCF

The photographs of displayed images using the MAMA-LCF on a color STN-LCD, PDLC, and Ch-LCD, taken under ambient condition are shown in the Fig. 17(a)–(c), respectively. In comparison, Fig. 17(a) is the photograph of STN-LCD with an MAMA-LCF (left) and an 80% haze diffuser (right), which is commonly used to enhance the brightness of mobile displays. The photographs of PDLC with MAMA light control film and a bare PDLC are shown in Fig. 17(b). Additionally, Fig. 17(c)

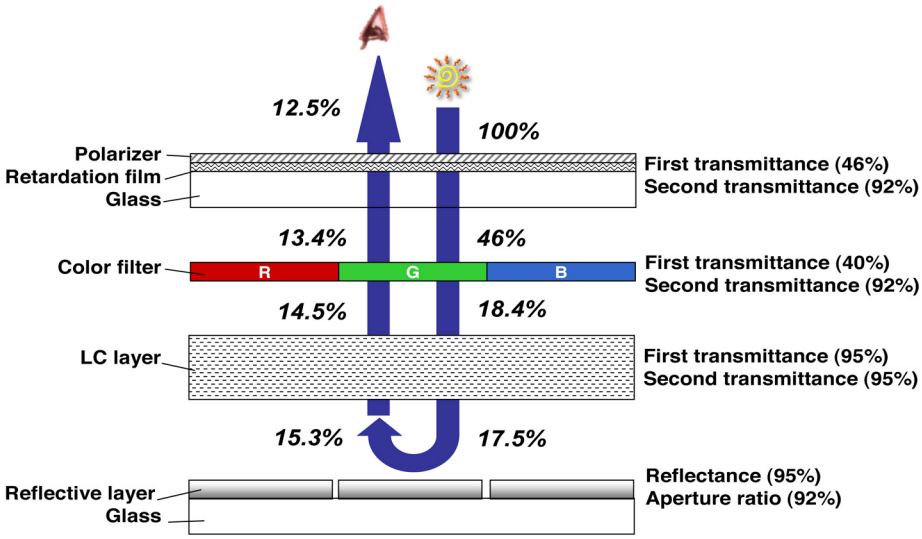

Fig. 14. Estimated reflective light efficiency of a reflective LCD. (Color version available online at http://ieeexplore.ieee.org.)

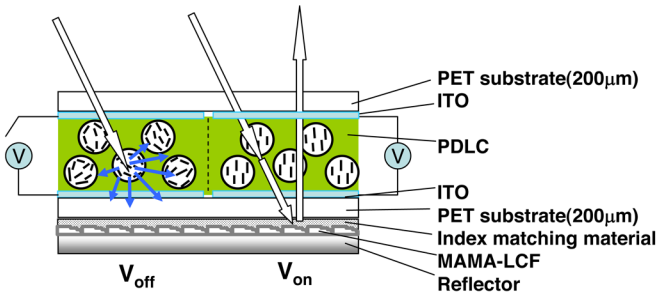

Fig. 15. Schematic plot of system configuration of the MAMA-LCF on a reflective PDLC. (Color version available online at http://ieeexplore.ieee.org.)

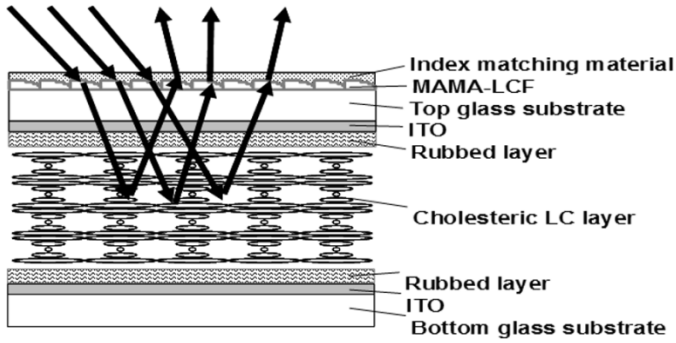

Fig. 16. Schematic plot of system configuration of the MAMA-LCF on a reflective cholesteric LCD.

displays the two-surface buffed Ch-LCD with and without MAMA-LCF, and also the photos of using MAMA-LCF on a conventional numerical TN panel by injected Ch-LC material, which reflected green and orange colors, respectively. The high image quality by the MAMA-LCF on the three different LCDs is clearly demonstrated.

F. Random Grating Light Control Film (RG-LCF)

RG-LCF, as shown in Fig. 18, which can direct light incident from multiple directions collectively for viewing, can achieve much enhanced brightness of reflective image. The grating pitches and orientations were designed properly to improve the brightness and uniformity. Additionally, the size of each grating is $25 \times 25\ \mu m^2$ and the arrangement in a single pixel is randomized in order to avoid the moiré patterns and dispersion.

A standard microfabrication and stamp molding processes can be used to fabricate the random grating structure on a 100 μm thick plastic thin foil economically. The fabricated grating structure imaged by AFM is shown in Fig. 19(a). The reflected light distribution of a transflective LCD with RG-LCF is shown as the solid line in Fig. 19(b), where the dashed lines show the specular reflection without the RG-LCF. Obviously, the transflective LCDs using LCF provides more uniform reflected light within typical viewing region from 0 to 25°, with higher reflectance and better image quality.

V. Image Enhanced Reflector

Reflective Ch-LCD is a strong contender for e-papers, e-books, etc. To enable a display to be usable from dark to bright sunlight conditions, transflective display is a good option. However, the conventional transflective approach does not apply to the cholesteric display. Both reflective and transmissive sub-pixels display bright state, but lack of dark state. We demonstrated a transflective Ch-LCD by placing an image-enhanced reflector (IER) above the transmissive part to reflect the backlight into the reflection pixels, as illustrated in Fig. 20 [15]. This IER design functions equally well for both monochrome and full color cholesteric displays. Due to the similar paths of transmissive and reflective light, the same bright state for both reflective and transmissive channels can be obtained. Thus, the Ch-LCD maintains good readability in any ambience.

The half-tone mask technology equipped with excimer laser micromachining was used to fabricate the prototype IER structure on a glass substrate, as shown in Fig. 21(a). Prior to examining the function of IER, we prepared a simple monochrome Ch-LCD test sample with conventional backlight. The images of reflective (left) and transmissive (right) mode are shown in Fig. 21(b). The photos successfully demonstrate that this novel transflective Ch-LCD can display same image color in any ambient condition by using microoptical component of IER.

Fig. 17. Sample photographs of: (a) color-STN LCD, (b) PDLC, and (c) Ch-LCD. The displays with MAMA-LCF clearly show much better image quality. (Color version available online at http://ieeexplore.ieee.org.)

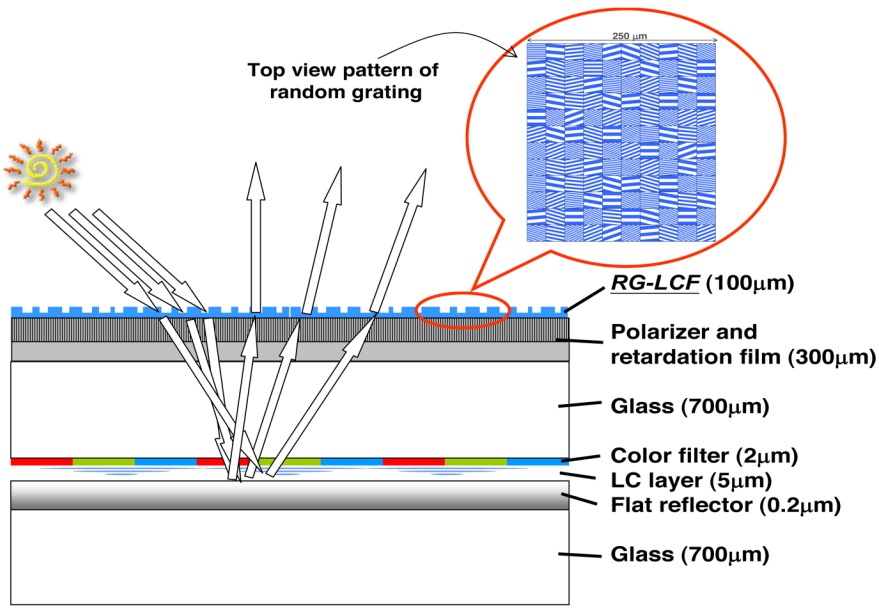

Fig. 18. Configuration of a TR-LCD with the RG-LCF laminated onto the front surface. (Color version available online at http://ieeexplore.ieee.org.)

VI. Microtube Array

In conventional transflective LCDs, the reflective area is regarded as a block that backlight can not pass through. In order to overcome the issue, a novel structure, micro-tube array, was proposed to collect the backlight into the transmissive area to increase light utilization efficiency of backlight in transflective LCDs. The characteristic of this design is to make use of a microoptical component of micro-tube structure which is similar to a funnel in shape and to allow most backlight enter this struc-

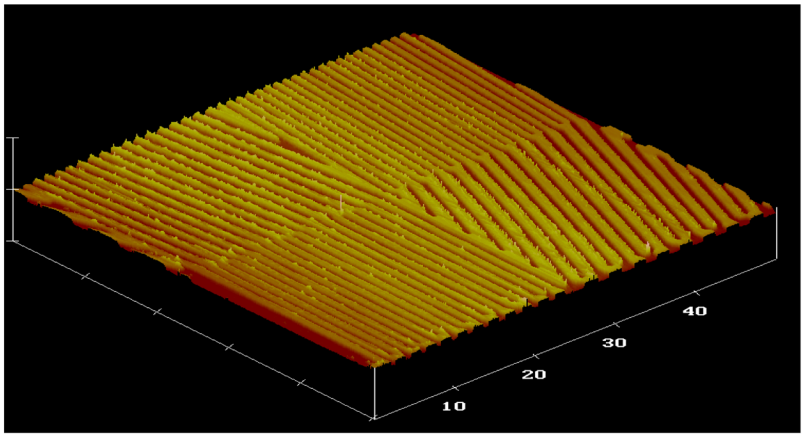

(a)

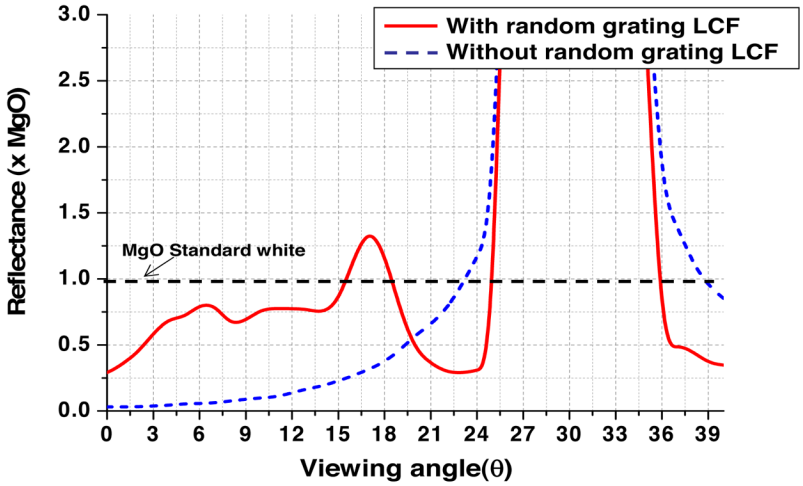

(b)

Fig. 19. (a) 3-D view and (b) the reflectance profile of the RG-LCF laminated on a TR-LCD. (Color version available online at http://ieeexplore.ieee.org.)

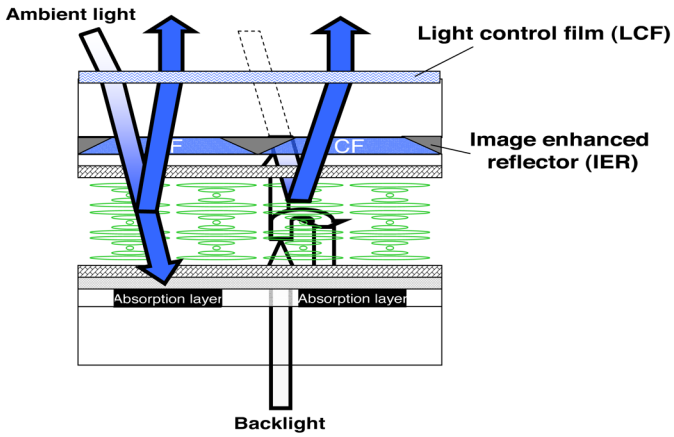

Fig. 20. Cross-sectional plot of the transflective Ch-LCD with an IER. (Color version available online at http://ieeexplore.ieee.org.)

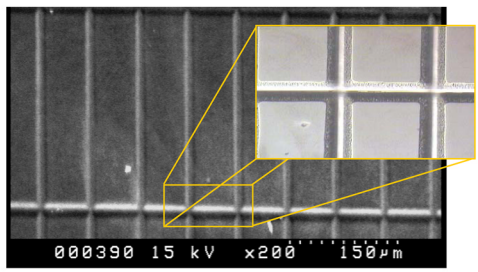

(a)

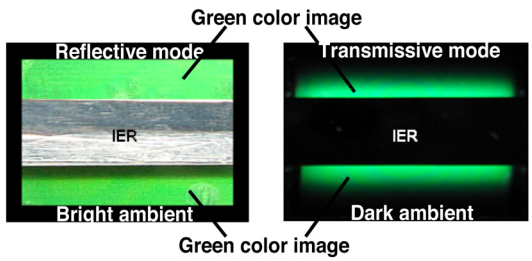

(b)

Fig. 21. (a) Top view of fabricated IER. (b) Demonstration photos of the same color images for both reflective and transmissive modes. (Color version available online at http://ieeexplore.ieee.org.)

ture from larger aperture, as shown in Fig. 22. On account of the characteristic of the funnel structure, most of incident light can be collected to smaller aperture so that light efficiency of the backlight can be increased substantially.

A prototype micro-tube array, as shown in Fig. 23(a), was fabricated by a typical TFT-LCD process. The measured transmissive light efficiency enhancement of micro-tube array structure is shown in Fig. 23(b). The measured enhancement in different viewing angle was a factor of 1.65 to 2.3, and the averaged enhancement was a factor of 1.81. As a result, the

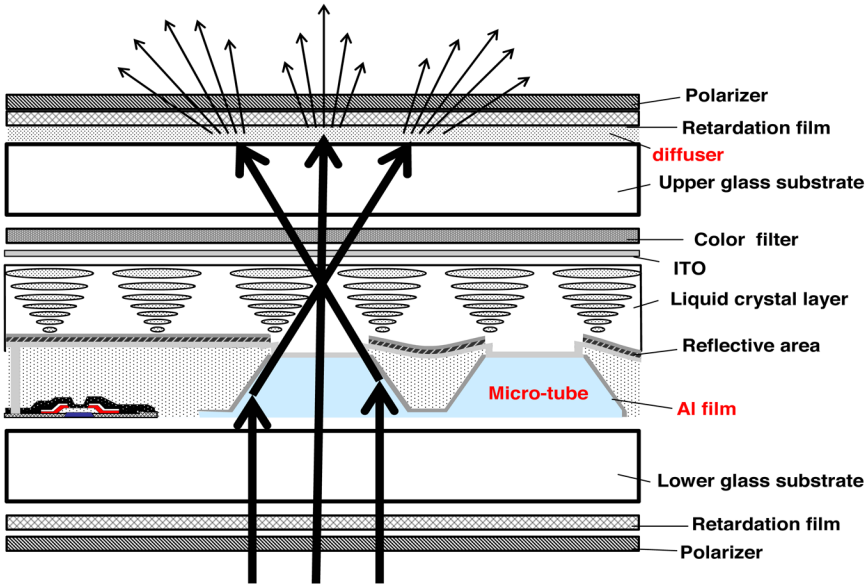

Fig. 22. Schematic diagram of a single cell-gap transflective LCD with micro-tube array. (Color version available online at http://ieeexplore.ieee.org.)

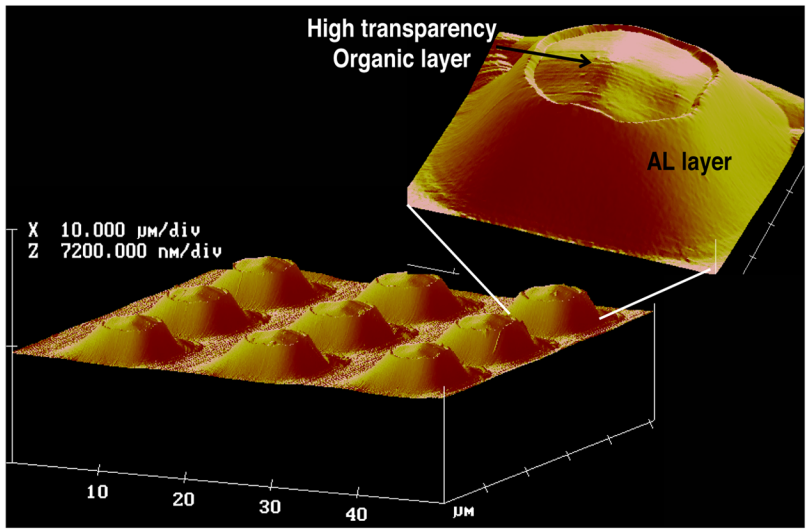

(a)

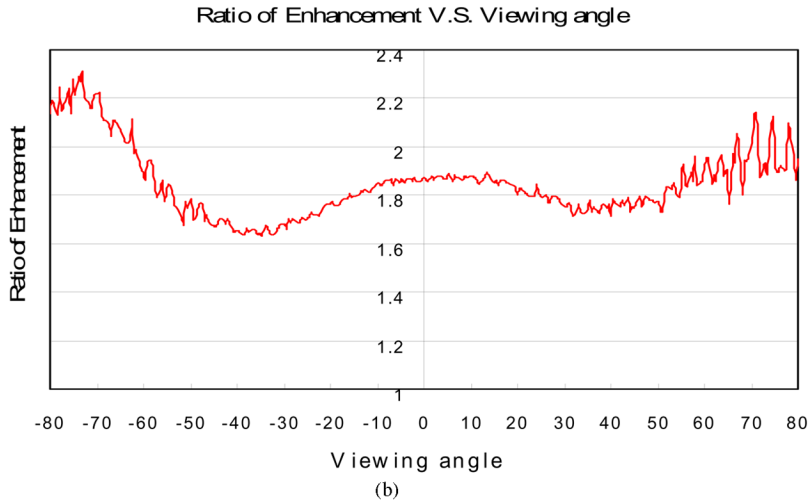

(b)

Fig. 23. (a) 3-D view and (b) the measured backlight efficiency enhancement plot. (Color version available online at http://ieeexplore.ieee.org.)

novel transflective LCDs with micro-tube array can be made with lower power consumption due to the higher backlight efficiency, which will be more competitive in the mobile display applications.

VII. Sub-Wavelength Grating

The optical efficiency of conventional backlight modules is low due to the lack of p-polarized to s-polarized light

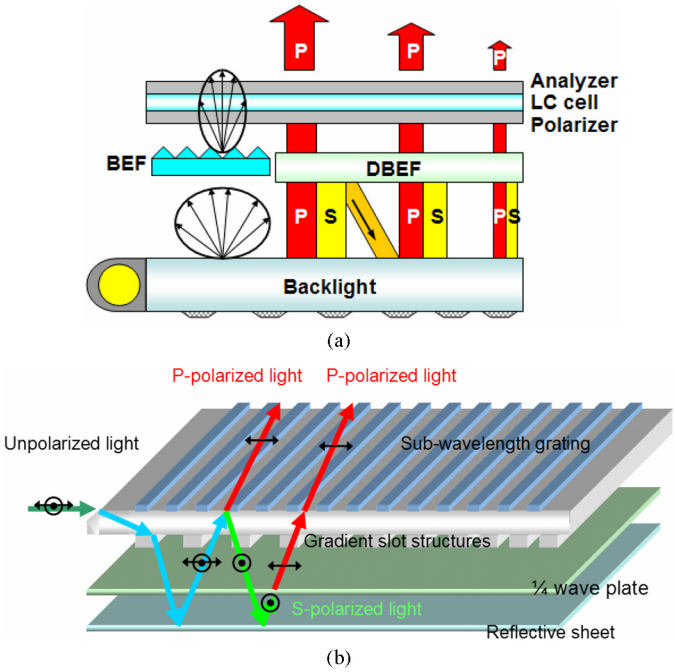

Fig. 24. Schematics of polarized backlights based on (a) selective T.I.R. and (b) sub-wavelength grating. (Color version available online at http://ieeexplore.ieee.org.)

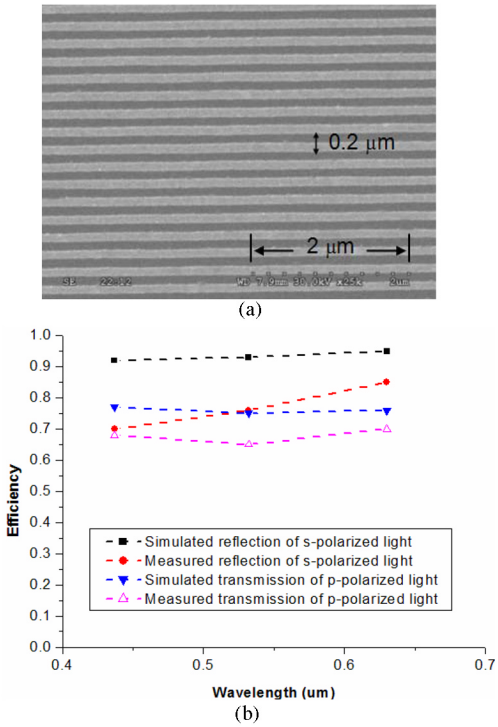

Fig. 25. (a) SEM photograph and (b) measured results of the sub-wavelength grating. (Color version available online at http://ieeexplore.ieee.org.)

conversion. Many approaches were reported to improve light efficiency. The most well-known approach is using Dual brightness enhancement film (DBEF) to recycle the undesired polarized light, as shown in Fig. 24(a) [16]. DBEF, which consists of a stack of alternate isotropic-birefringent films, can reflect the complimentary light which polarized in the direction of the extraordinary axis. The reflected polarized light is again reflected by a depolarizing reflector. However, the complex assembling and high cost of optical films, such as brightness enhancement film (BEF), DBEF, and diffuser, usually hinders compact packaging.

An integrated backlight using sub-wavelength grating was, therefore, proposed to achieve polarization conversion and compactness for LCD illumination, as shown in Fig. 24(b), [17]. When unpolarized light was coupled to the lightguide, slot structures on the bottom surface guided light outcoupling. Light was then reflected by the reflective sheet. Upon the impingement on the sub-wavelength grating on the top surface, only p-polarized light was transmitted while s-polarized light was reflected. S-polarized light was then converted into p-polarized light by passing through the quarter wave plate twice. The sub-wavelength grating consists of Al (100-nm thick) and SiO_2 (200-nm thick) layers with 0.2 μm period of 50% duty cycle. Moreover, the sub-wavelength grating is not so critical on incident angle. Therefore, outcoupling light was uni-polarized, which was required for LCD illumination.

The fabricated pattern of sub-wavelength grating is presented in Fig. 25(a). The transmission and reflection of fabricated sub-wavelength grating were measured by a white light source accompanied with R (630 nm), G (532 nm), B (437 nm) three primary wavelength color filters. The measured and simulated reflection efficiencies versus wavelength are shown in Fig. 25(b).

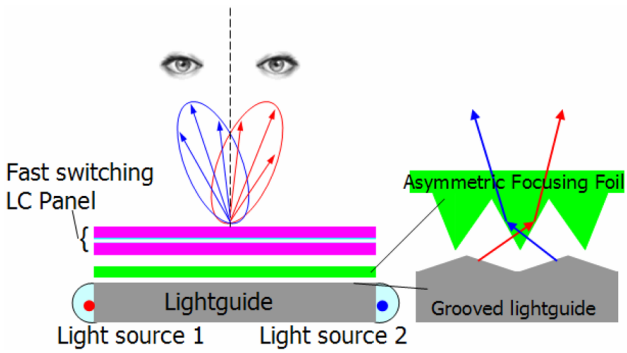

Fig. 26. Micro-grooved lightguide in combination with a focusing foil to redirect light to left and right eyes. (Color version available online at http://ieeexplore.ieee.org.)

In such an arrangement, the measured reflection efficiencies at $\lambda = 437, 532$, and 630 nm are 70%, 76% and 85% for s-polarized light; transmission efficiencies for p-polarized light are 68%, 65% and 70%, respectively. Thus, gain factor of 1.7 in polarization efficiency was yielded compared with conventional backlights, which increases utilization light for LC illumination.

VIII. Grooved-Lightguide With Focusing Foil

Autostereoscopic 3-D display can be generally classified into "spatial-multiplexed type" and "time-multiplexed type". Using parallax barrier [18] and lenticular lens are the most popular spatial-multiplexed approaches to obtain two emitting cones of light to respective eyes, yet, resulting in resolution of one half or less and light efficiency degradation compared to time-multiplexed approach. Furthermore, critical alignment to LCD pixels is a serious concern.

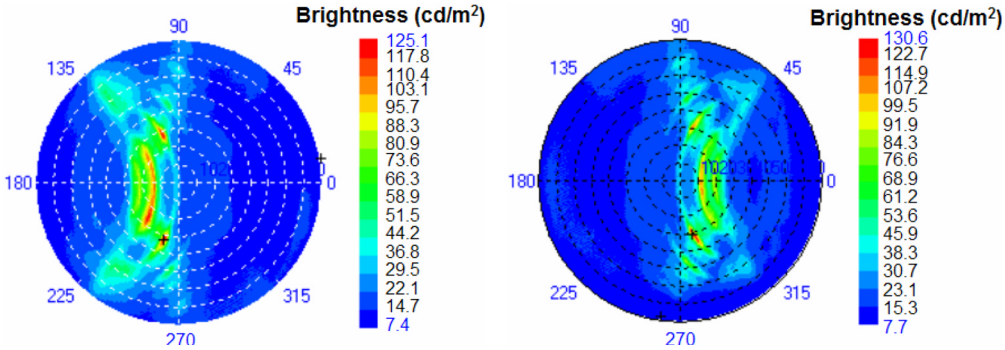

(a) (b)

Fig. 27. Angular distributions of the backlight module with LC panel when (a) left and (b) right side LEDs are switched on. (Color version available online at http://ieeexplore.ieee.org.)

Therefore, we demonstrated a switching, directional backlight in combination with fast switching LCD to realize time-multiplexed 3-D displays [19]. Two restricted viewing cones were sequentially emitted from switching backlights. Two sets of light sources were switched on sequentially to emit light to the left and the right eyes, respectively. A directional backlight, shown in Fig. 26, is composed of a micro-grooved lightguide in combination with a focusing foil. When the light source was switched on, a large inclined angle of viewing cone was emitted from a micro-grooved lightguide. In order to focus the light by the desired viewing angles, a focusing foil, which consists of asymmetric grooves, was then utilized to redirect the light to the eyes.

Observers left and right eyes were typically located around -10° and 10° to the normal direction of the display, respectively. For backlight brightness intensity of 2100 cd/m^2, Fig. 27(a) and (b) depicts the measured angular distributions of directional backlight with LC panel by sequentially switching the left and right side LEDs. For $\phi' = 90^\circ$ cross-section, the measured luminous intensity is 109 cd/m^2 at viewing angle of -10° (left eye) while 7 cd/m^2 at viewing angle of 10° (right eye). In the measurement, crosstalk is of approximately 6%. Additionally, when our left eye is located at viewing angle between -7.5° and -20° while our right eye at viewing angle between 7.5° and 20°, crosstalk is of less than 10%, which is the minimum criterion to produce stereoscopic image perception for our brain. The position of viewer can be moved within the range of viewing angle between -7.5° and -20°. Therefore, the viewing distance can be adjusted within 90 and 250 mm.

Furthermore, 2-D/3-D compatibility is provided by switching on two sets of light sources simultaneously or sequentially, respectively. 2-D image perception is achieved when there is no binocular disparity while simultaneously observing the same image. In contrast, 3-D image perception is obtained by combining sequentially switching images in our brain.

IX. Conclusion

Micro-optics can meet the needs of miniaturization, cost reduction, and improved performance in LCDs. Design consideration and fabrication processes were described for microoptical components used for LCDs. MAMA-LCF and (RG-LCF enhance the reflectance of reflective image to 0.8x MgO standard white with excellent uniformity. IER provides transflective function for Ch-LCDs, which become readable in any ambience. Micro-tube array increases the backlight utilization to a factor of 1.8 in transflective LCDs. Sub-wavelength gating almost doubles the backlight efficiency. Furthermore, grooved-lightguide with focusing foil using switchable backlight generates the 2-D images into 3-D images. Accordingly, the microoptical technology can greatly enhance the image quality of display systems, and allows the display to be more and more appealing and attractive in various applications.

References

[1] H. P. Herzig, *Micro-Optics Elements, System, and Applications*. New York: Taylor & Francis, 1998.
[2] *Handbook of Display Technology*, Academic, San Diego, CA, 1992. J. A. Castellano.
[3] B. E. A. Saleh and M. C. Teich, *Fundamental of Photonics*. New York: Wiley, 1991.
[4] M. Oikawa and K. Iga, "Distributed-index planar microlens," *Appl. Opt.*, vol. 21, pp. 1052–1056, Mar. 1982.
[5] N. F. Borelli, D. L. Morse, R. H. Bellman, and W. L. Morgan, "Micro lens arrays produced by photolytic technique," *Appl. Opt.*, vol. 27, pp. 476–479, Feb. 1988.
[6] A. J. Stevens, W. J. Hossack, and S. Samus, "Very-large-scale-integration fabrication technique for binary-phase gratings on sapphire," *Appl. Opt.*, vol. 34, pp. 190–193, Jan. 1995.
[7] J. N. Mait, "Understanding diffractive optic design in the scalar domain," *J. Opt. Soc. Amer. A.*, vol. 12, pp. 2145–2158, Oct. 1995.
[8] J. Jahns and S. J. Walker, "Two-dimensional array of diffractive microlenses fabricated by thin film deposition," *Appl. Opt.*, vol. 29, pp. 931–936, Mar. 1990.
[9] Y. Itoh, S. Fujiwara, N. Kimura, S. Mizushima, F. Funada, and M. Hijikigawa, "Influence of rough surface on the optical characteristics of reflective LCD with a polarizer," in *Proc. SID'98*, 1998, pp. 221–224.
[10] D. L. Ting, W. C. Chang, C. Y. Liu, J. W. Shiu, C. J. Wen, C. H. Chao, L. S. Chuang, and C. C. Chang, "A high-brightness high-contrast reflective LCD with a micro slant reflector (MSR)," in *Proc. SID'99*, 1999, pp. 954–957.
[11] F. J. Ko and H. P. D. Shieh, "Brightness and contrast enhancement of reflective liquid crystal displays by microlens array light control film," *Jpn. J. Appl. Phys.*, vol. 39, pp. 2647–2650, May 2000.
[12] Y. P. Huang, J. J. Chen, F. J. Ko, and H. P. D. Shieh, "Multidirectional asymmetrical microlens array light control film for improved image in reflective color liquid crystal displays," *Jpn. J. Appl. Phys.*, vol. 41, pp. 646–651, Feb. 2002.
[13] Y. P. Huang, H. P. D. Shieh, and S. T. Wu, "Applications of multidirectional asymmetrical microlens-array light-control films on reflective liquid-crystal displays for image quality enhancement," *Appl. Opt.*, vol. 43, pp. 3656–3663, Jun. 2004.
[14] G. R. Fowles, *Introduction to Modern Optics*, 2nd ed. New York: Holt, Rinehart, and Winston, 1975, ch. 2.
[15] Y. P. Huang, X. Y. Zhu, H. W. Ren, Q. Hong, T. X. H. Wu, S. T. Wu, S. H. Lin, and H. P. D. Shieh, "Full-color transflective Ch-LCD with image-enhancement reflector," *SID'04*, pp. 882–885, 2004.
[16] E. Lueder, *Liquid Crystal Displays*: Wiley, 2000, pp. 294–298.

[17] K. W. Chien and H. P. D. Shieh, "Design and fabrication of an integrated polarized light guide for liquid-crystal-display illumination," *Appl. Opt.*, vol. 43, no. 9, pp. 1830–1834, Mar. 2004.
[18] I. Sexton, "Parallax barrier 3-D TV," *SPIE Proc.*, vol. 1083, pp. 84–91, Jan. 1989.
[19] K. W. Chien and H. P. D. Shieh, "3D mobile display based on sequentially switching backlight with focusing foil," in *SID'04*, 2004, pp. 1434–1437.

Han-Ping D. Shieh received the B.S. degree from National Taiwan University in 1975 and Ph.D. degree in electrical and computer engineering from Carnegie Mellon University, Pittsburgh, PA, in 1987.

From 1988, he had been a Research Staff Member at IBM TJ Watson Research Center, Yorktown Heights, NY . In 1992, he joined National Chiao Tung University (NCTU) in Hsinchu, Taiwan, R.O.C., as a professor at Institute of Opto-Electronic Engineering and Microelectronics and Information Research Center (MIRC). He is currently AU Optronics chair professor and Associate Director, MIRC, NCTU. Hehad founded and served as the director of Display Institute at NCTU in 2003, the first such kind of graduate academic institute in the world dedicated for display education and research. He also holds a joint-appointment as a Research Fellow at Center for Applied Sciences and Engineering, Academia Sinica since 1999. His current research interests are in display, optical MEMS, nano-optical components, and optical data storage technologies. He has published more than 100 journal papers and has more 30 patents to his credit.

Dr. Shieh currently serves as a Director, SID (Society for Information Display), and has served as program chair, committee member, organized conferences in major data storage (ISOM, MORIS, Intermag, ODS, APDSC) and display (SID, IDRC, ASID, FPD Expo, etc.). He was elected as a Society for Information Display (SID) fellow in 2005.

Yi-Pai Huang received the B.S. degree from National Cheng-Kung University in 1999 and the Ph.D. degree from National Chiao-Tung University, Hsinchu, Taiwan, R.O.C., in 2004.

He now is a senior engineer of AU Optronics Corporation, Hsinchu, Taiwan, R.O.C. His current research interests and projects are reflective and transflective displays, microoptical design and fabrication, and wide viewing angle LCDs.

Dr. Huang was awarded the SID 2001 Best Student Paper Award and a SID 2004 distinguished student paper.

Ko-Wei Chien received the B.S. degree from National Tsing-Hua University in 1999, and joined the Ph.D. program of the Institute of Opto-Electronic Engineering, National Chiao Tung University (NCTU) , with merit. He is currently working toward the Ph.D. degree in NCTU.

He had joined the group of Flat Display Modules, Philips National Laboratory as an internship student in 2003. His current research interests are transmissive displays, backlight module design, microoptical design and fabrication, and 3-D displays.